Proceedings of the ASME 2021
International Mechanical Engineering Congress and Exposition
IMECE2021
November 1-5, 2021, Virtual, Online

IMECE2021-67839

CHARACTERIZATION OF LATERAL FRICTION SURFACED AA6063 COATINGS

Ebrahim Seidi*, Scott F. Miller
Department of Mechanical Engineering, University of Hawaii at Manoa
Honolulu, Hawaii, USA
*seidi@hawaii.edu

ABSTRACT

Friction surfacing is a solid-state metal deposition technique suitable for a wide range of metallic materials. This technique results in coatings on surfaces for joining purposes or surface modification applications such as wear and corrosion performance improvements. In this study, a novel approach in friction surfacing is utilized in which the consumable tool deposits material from its side instead of the end of the tool, which has been employed in conventional friction surfacing. Frictional heat enables plastic deformation, which results in the depositing of the consumable material on the substrate surface. The process is carried out at temperatures below the melting point of the consumable material, resulting in a solid-state deposition process. In the current study, scanning electron microscopy and energy dispersive spectroscopy have been employed for the characterization of the interfaces and coatings. The results of this study exhibited that there is no elemental diffusion between the tool and substrate materials at the interface, showing that the process temperature was low enough to prevent plasticizing of the substrate surface.

Keywords: Friction Deposition, Lateral Friction Surfacing, Side of the Tool, Characterization, SEM, EDS

1. INTRODUCTION

The friction surfacing (FS) technique is a friction-based approach, suitable for fabricating solid-state deposits using a rotating consumable rod. The tool is forged onto the surface of a substrate along its axis, and due to the frictional heat generated at the tool/substrate interface, the consumable material plasticizes and sheared on the substrate surface [1]. Several important process factors such as pressing force, table traverse speed, spindle speed, and tool/substrate materials significantly impact on the quality of resulting deposits. Therefore, these parameters can be utilized as the controlling process factors to achieve the desired quality. Moreover, several studies exhibited that by adding reinforcing particles into the holes drilled through the consumable rod, the FS can be utilized for other purposes such as surface hardening, and improving the wear and corrosion performance of the surfaces [2-8]. The influences of process factors on the deposit width and thickness have been investigated in several studies [9-14].

FS technique can develop metallic deposits at temperatures less than melting points of tool/substrate materials, followed by a rapid cooling process, which makes this method an excellent approach for fabricating fine-grained deposits [15]. There is a need to investigate the microstructural development and material properties after a high rate of deformation experienced by consumable material during the FS process. Several different kinds of analyses such as optical microscopy [16], scanning electron microscopy (SEM) [16], X-ray diffraction [9, 16], energy dispersive spectroscopy (EDS) [17, 18], hardness testing [19-22], surface roughness testing [23-25], tensile testing [22] have been performed to study the coating quality.

Lateral friction surfacing (LFS), a novel technique derived from the conventional FS approach, can be employed to fabricate deposit layers. In this approach, instead of the consumable rod end face, the side of the rod is forced onto the substrate surface, resulting in material deposition from the radial surface of the tool, as presented in Fig. 1. LFS approach can provide ultra-smooth and thin deposits compared to the conventional FS technique. Moreover, the coating fabricated in this technique is more consistent since there is no advancing or retreating side on the deposits, and all points on the fabricated deposits at the tool/substrate interface experience the same constant rotational speed. Unlike the conventional FS technique, the LFS approach creates no flash; therefore, it is capable of saving a significant amount of consumable materials and increase economic efficiency. Furthermore, this technique generates lower process temperatures compared to the conventional approach, which helps to reduce the thermal impacts on the metallurgical and mechanical properties of the coatings.

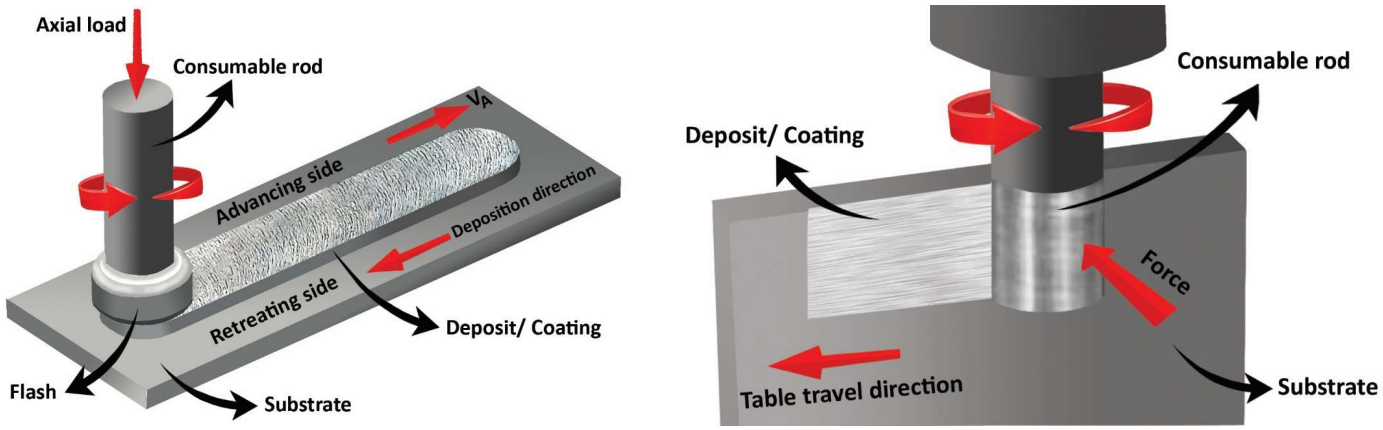

FIGURE 1: SCHEMATIC OF (LEFT) CONVENTIONAL FS (RIGHT) THE NOVEL APPROACH OF LFS [27]

The LFS of AA6063 consumable tool onto A36 carbon steel was investigated in [26]. Several combinations of process factors and also single and double-pass deposition approaches were employed to evaluate their impacts on the quality, thickness, coverage, and surface roughness of the deposits. This study is an attempt to characterize the lateral friction surfaced AA6063 coatings fabricated in [27], which were previously subjected to different analyses such as surface roughness measurement, material deposition rate measurement, force measurement, infrared thermography, and optical microscopy.

2. MATERIALS AND METHODS

In this study, the material composition of the coatings fabricated through the LFS process was characterized. To provide the required samples, LFS of AA6063 onto AISI 1018 carbon steel was performed using a JET JMD-18 milling machine. AA6063 consumable rods with a length of 100 mm and a diameter of 12.7 mm, and AISI 1018 substrates with dimensions of 127 mm × 63.5 mm × 3.175 mm were utilized. The chemical composition of consumable rod and substrate materials are presented in Tables 1 and 2, respectively [28]. The various process parameters such as applied forces of 150 and 250 N, spindle speeds of 2300 and 3000 rpm, and a constant traverse speed of 76.2 mm/min were employed, as summarized in Table 3. The applied forces were controlled manually during the process using a dynamometer and LabVIEW programming. As shown in Fig. 2, 1 cm of the deposited coatings were cut and mounted in epoxy, and then the specimens were polished using 1 and 0.3 µm alpha-alumina for cross-sectional SEM and EDS analyses.

TABLE 1. CHEMICAL COMPOSITION OF AA6063-T5 ALUMINUM ALLOY

Materials	**Mg**	**Si**	**Cr**	**Cu**	**Mn**	**Ti**	**Zn**	**Fe**	**Al**
% of composition	0.45-0.9	0.2-0.6	≤ 0.1	≤ 0.1	≤ 0.1	≤ 0.1	≤ 0.1	≤ 0.35	Balance
Physical Property	**Melting Point**		**UTS**		**Elongation at Break**			**Thermal Conductivity**	
Values	616°C		186 MPa		22% @ 24.0°C			209 W/m.K	

TABLE 2. CHEMICAL COMPOSITION OF AISI 1018

Materials	**Mn**	**P**	**S**	**C**	**Fe**
% of composition	0.60 - 0.90	≤ 0.040	≤ 0.050	0.14 - 0.20	98.81 - 99.26
Physical Property	**Melting Point**	**UTS**	**Elongation at Break**		**Thermal Conductivity**
Values	1480°C	440 MPa	15 % @ 24.0°C		51.9 W/mK

TABLE 3. PROCESS PARAMETERS EMPLOYED IN THE LFS PROCESSES

Sample Number	**Tool Rotational Speed (rpm)**	**Force (N)**	**Traverse Speed (mm/min)**
1	2300	150	76.2
2	2300	250	76.2
3	3000	150	76.2
4	3000	250	76.2

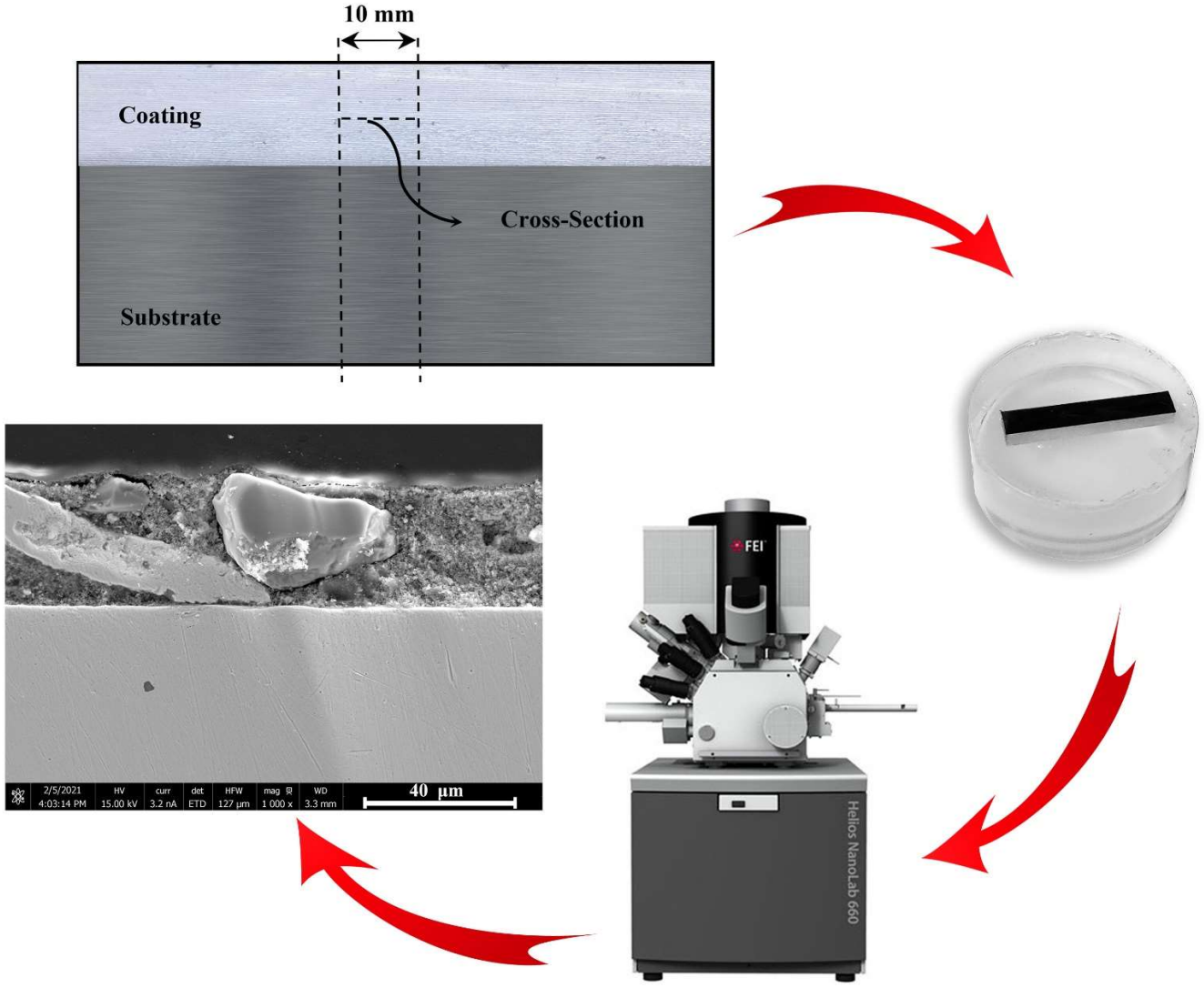

FIGURE 2: CROSS-SECTIONING OF THE DEPOSITS

The deposits and their interfaces with the substrate were investigated by a FEI Helios NanoLab 660 Dual-Beam SEM-FIB equipped with an Oxford Instruments X-Max EDS detector. The SEM analysis was done to qualify the coating in terms of cracks in the coatings, and intermixing and diffusion of consumable rod and substrate materials. The EDS maps of the cross-sections were provided to illustrate the Al, Si, O, C, Fe, and Mn elemental distributions in the coating and substrate.

3. Results

The fabricated deposits using LFS were subjected to SEM and EDS analyses. Two different magnifications for the SEM imaging were employed. The lower magnification shows the consistency of the coatings, and higher magnification provides a detailed visual assessment of the substrate/coating interface including cracks and porosity in the deposits, as shown in Figs. (3-6). Process parameter values of pressing force and spindle speeds have an effect on the number of cracks and pores, coating thickness, and coating surface roughness.

The SEM and EDS analyses of the deposited coating using the pressing force of 150 N and spindle speed of 2300 rpm are presented in Fig. 3. The SEM imaging using lower magnification shows a consistent and smooth coating; however, the higher magnifications revealed the presence of several cracks inside the coating layer. It was shown there are unbonded regions at the substrate/coating interface, as well as several cracks close to the interface, which could weaken the bonding between the coating and substrate.

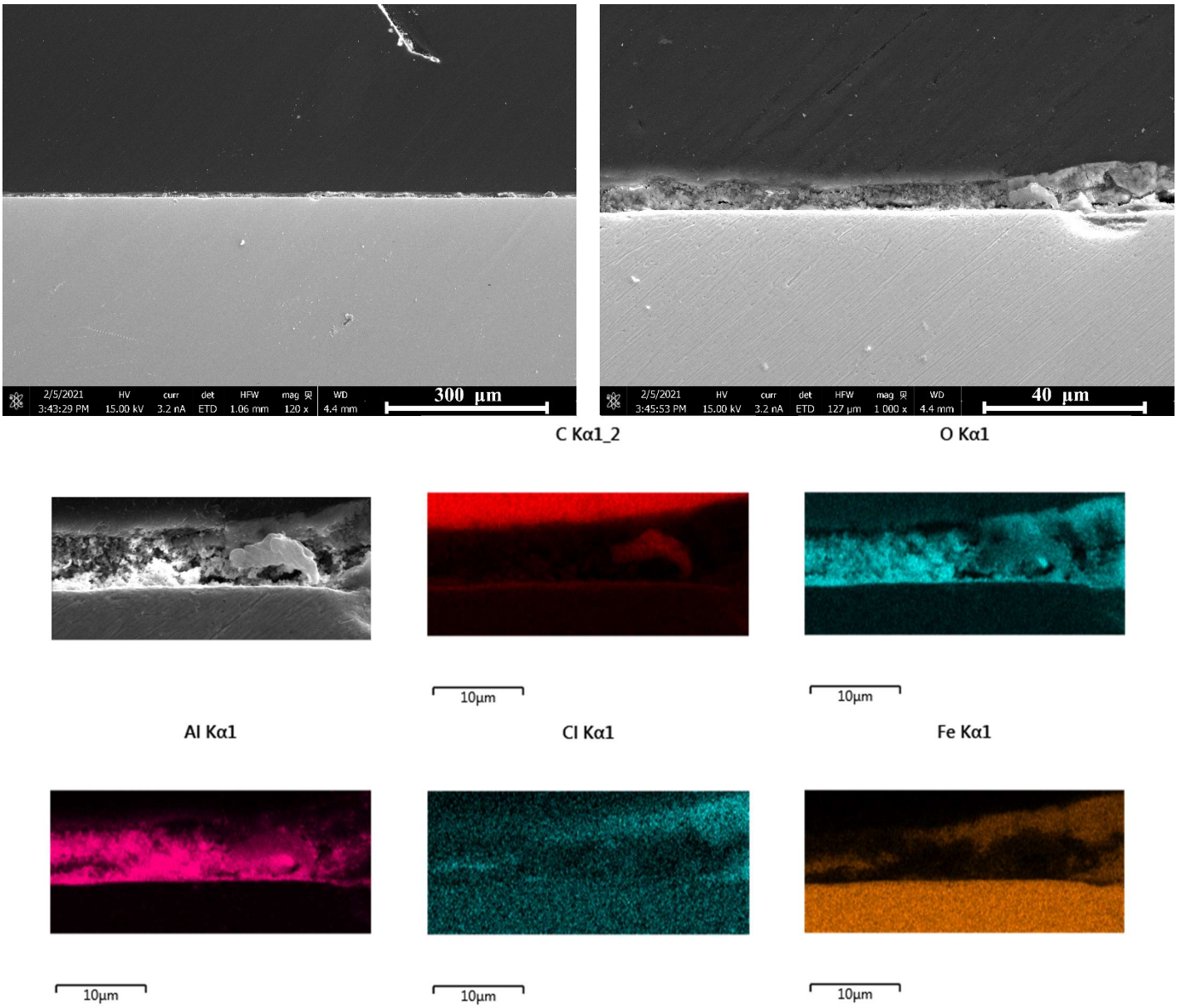

FIGURE 3: SAMPLE #1: 2300 RPM, 150 N

The SEM images and EDS maps of the coating deposited by spindle speed of 2300 rpm and normal force of 250 N are shown in Fig. 4. The SEM analysis using lower magnification shows that increasing the normal force from 150 N to 250 N, significantly increases the coating thickness and results in a rough deposit compared to sample 1. It appears that the aluminum was sheared onto the substrate in ~100 µm layers repeating every ~600 µm of tool travel. Small voids can be seen at the end where the layers did not fully adhere together at the top micrograph in Fig. 4. The higher magnifications employed in the SEM analysis revealed the absence of cracks inside the coating and a good bonding at the substrate/coating interface; however, few small pores were observed within the deposit. Moreover, there was less Fe detected with these settings.

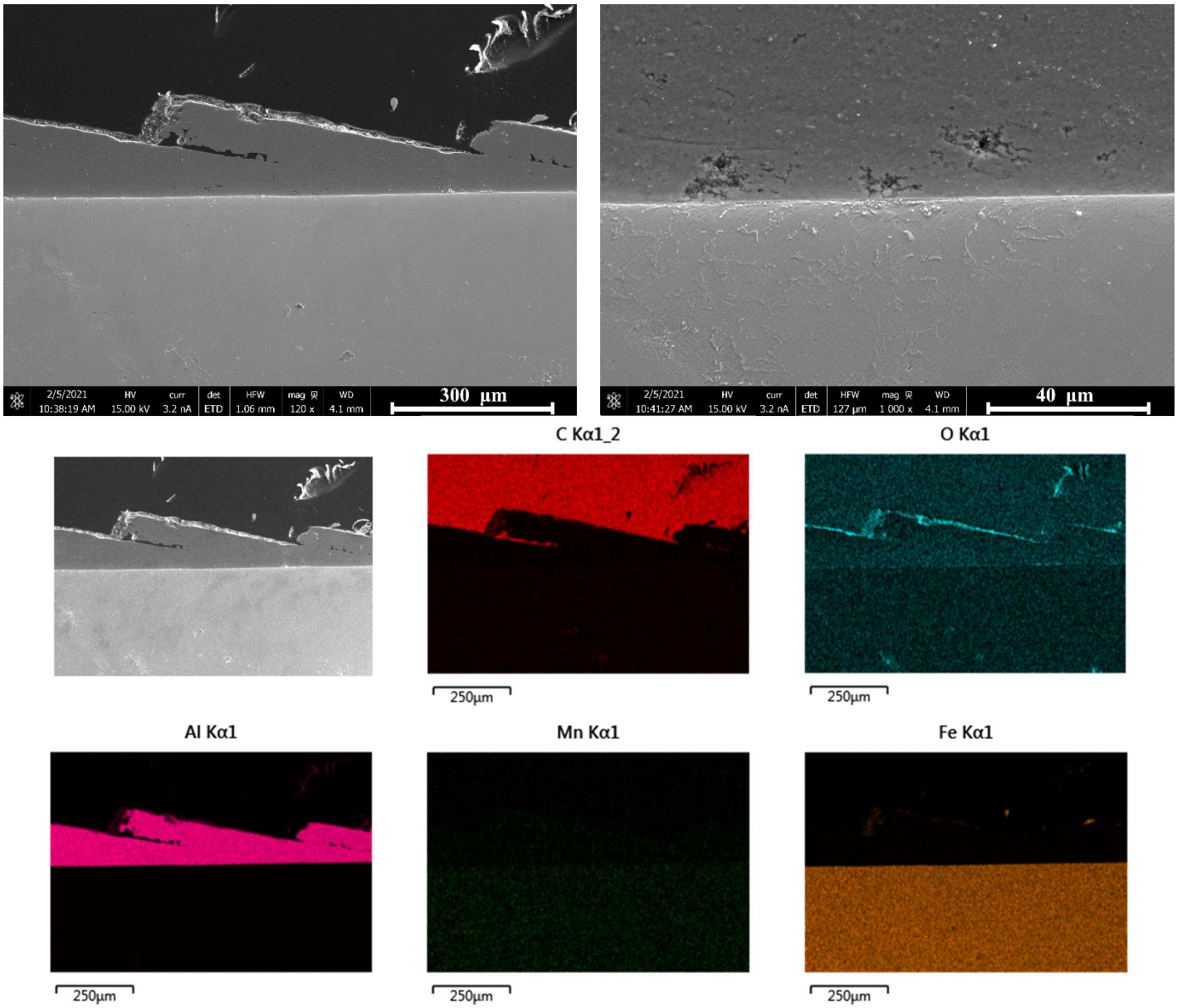

FIGURE 4: SAMPLE #2: 2300 RPM, 250 N

Fig. 5 exhibits a uniform coating thickness fabricated by spindle speed of 3000 rpm and normal force of 150 N. A coating free of cracks with a complete bonding at the substrate/coating interface were observed. The EDS maps show that excess Si in the plasticized consumable material results in large Si-rich particles forming in the coating. The formation of these kinds of particles negatively impacts the formability of the deposits and can result in cracking and reduced bonding and corrosion performance.

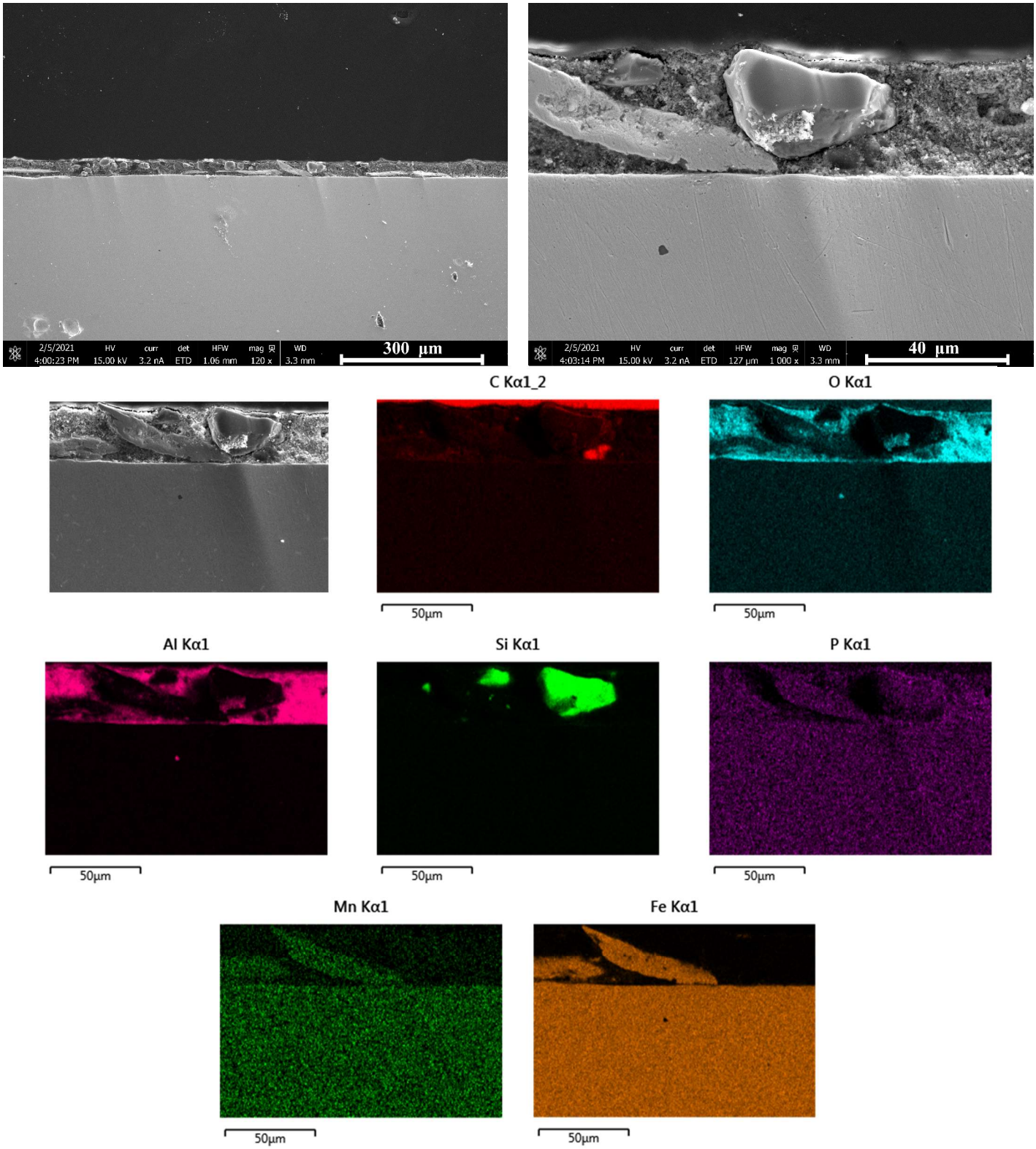

FIGURE 5: SAMPLE #3: 3000 RPM, 150 N

The SEM images and EDS maps presented in Fig. 6 present detailed cross-sectional viewing of the coating, interface, and the elemental distribution in the coating layer deposited by the normal force of 250 N and spindle speed of 3000 rpm. It was revealed that employing these values for process parameters results in significantly more cracks and porosities inside the

deposit. Moreover, few Si-rich regions were observed in the coatings, which are smaller than those in sample 2.

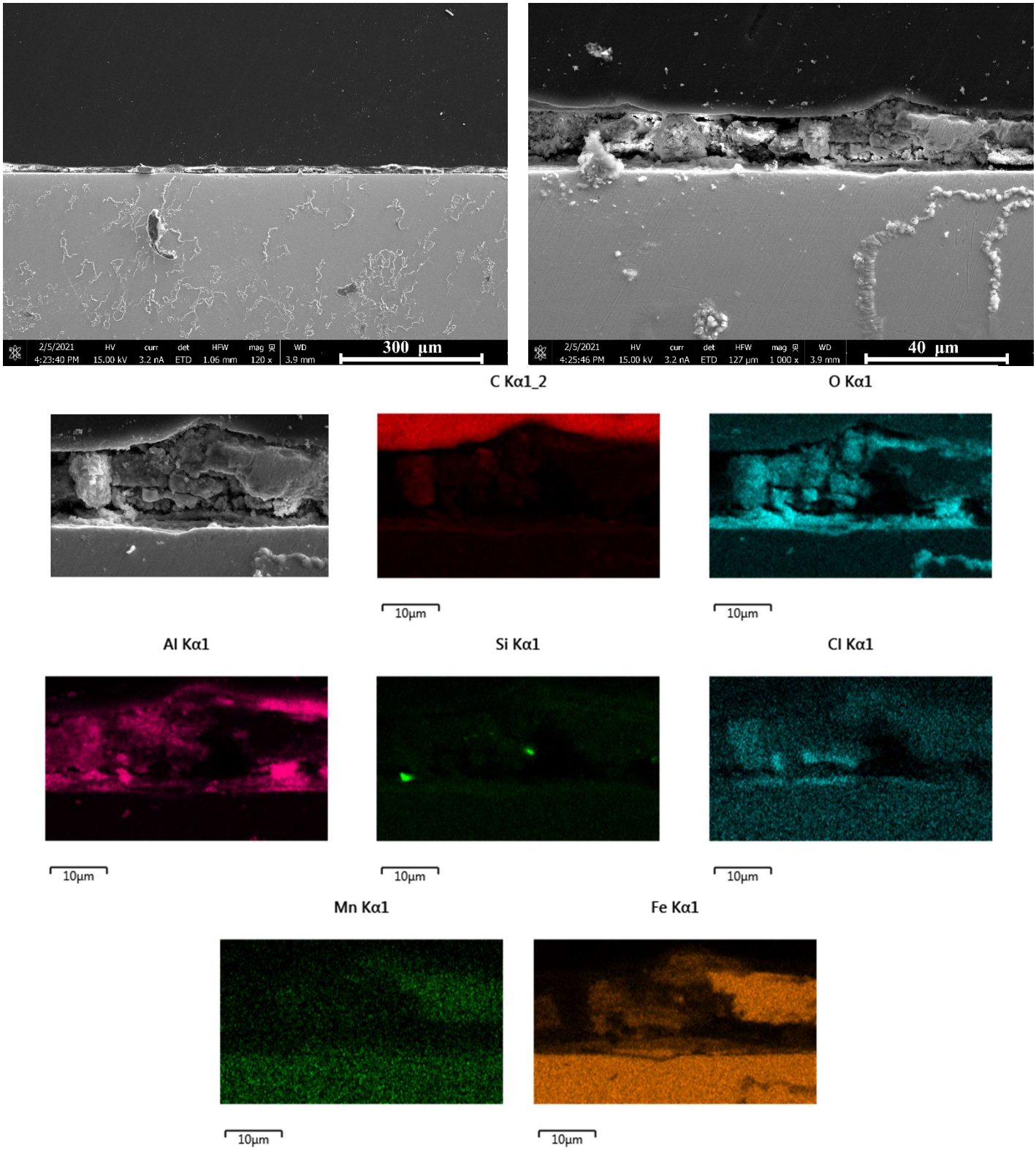

FIGURE 6: SAMPLE #4: 3000 RPM, 250 N

In all the specimens, oxidation was observed in the substrate material and more severely in the aluminum coatings. This phenomenon was revealed by the EDS maps, showing the presence of oxygen everywhere, especially on the cross-sectioned aluminum coatings. Moreover, the presence of a large amount of Fe in most samples shows that the substrate material was rubbed off due to the high spindle speeds and applied forces during the LFS process, resulting in transferring the substrate material's elements to the deposits.

4. Conclusion

In this investigation, AA6063 coatings fabricated by different process factors through LFS process were characterized. For this purpose, cross-sectional SEM and EDS analyses were employed for a detailed assessment of the coatings and the interfaces. The SEM analysis exhibited the presence of more cracks and porosities in the coatings fabricated by higher values of spindle speed and applied force. The coating deposited by 2300 rpm and 250 N exhibits lower cracks and porosities; however, it has an inconsistent coating thickness. The EDS maps show that excess Si in the plasticized consumable material results in large Si-rich particles forming in at least one sample. The formation of these kinds of particles negatively impacts the formability of the deposits and can result in cracking and reduced corrosion performance. Moreover, the EDS analysis revealed the presence of a large amount of Fe in most of the samples, indicating that the substrate material was rubbed off during the LFS process, and the substrate material was transferred to the deposits.

ACKNOWLEDGMENTS

This investigation was supported by NSF CMMI grant # 1763147 and General Motors.

REFERENCES:

[1] Seidi, E., and Miller, S. F., 2019, "Friction Surfacing Using Consumable Tools: A Review," Proceedings of the ASME 2019 14th International Manufacturing Science and Engineering Conference. Volume 2: Processes; Materials. Erie, Pennsylvania, USA. June 10–14, V002T03A048.
https://doi.org/10.1115/MSEC2019-2963

[2] Badheka, K., and Badheka, V. J., 2019, "Wear Behaviour of Boron Carbide Added Friction Surfaced Cladded Layer," Layer. In: Deb D., Balas V., Dey R. (eds) Innovations in Infrastructure. Advances in Intelligent Systems and Computing, 757, pp. 395-406.
https://doi.org/10.1007/978-981-13-1966-2_35

[3] Guo, D., Kwok, C. T., and Chan, S. L. I., 2018, "Fabrication of stainless steel 316L/TiB2 composite coating via friction surfacing," Surface and Coatings Technology, 350, pp. 936-948.
https://doi.org/10.1016/j.surfcoat.2018.03.065

[4] Pirhayati, P., and Aval, H. J., 2019, "Effect of silver on non-isothermal aging of friction surfaced AA2024-16 wt% Ag composites," Surface and Coatings Technology, 379, 125059.
https://doi.org/10.1016/j.surfcoat.2019.125059

[5] Oliveira, P. H. F., Galvis, J. C., Martins, J. D. P., and Carvalho, A. L. M., 2017, "Application of friction surfacing to the production of aluminum coatings reinforced with Al2O3 particles," Materials Research, 20, pp. 603-620.
https://doi.org/10.1590/1980-5373-mr-2017-0039

[6] Karthik, G. M., Ram, G. J., and Kottada, R. S., 2016, "Friction deposition of titanium particle reinforced aluminum matrix composites," Materials Science and Engineering, A, 653, pp. 71-83.
https://doi.org/10.1016/j.msea.2015.12.005

[7] Belei, C., Fitseva, V., Dos Santos, J. F., Alcântara, N. G., and Hanke, S., 2017, "TiC particle reinforced Ti-6Al-4V friction surfacing coatings," Surface and Coatings Technology, 329, pp. 163-173.
https://doi.org/10.1016/j.surfcoat.2017.09.050

[8] Miranda, R. M., Santos, T. G., Gandra, J., Lopes, N., and Silva, R. J. C., 2013, "Reinforcement strategies for producing functionally graded materials by friction stir processing in aluminium alloys," Journal of Materials Processing Technology, 213(9), pp. 1609-1615.
https://doi.org/10.1016/j.jmatprotec.2013.03.022

[9] Sahoo, D. K., and Mohanty, B. S., 2019, "Evaluation of Bond Strength on Deposition of Aluminium 6063 Alloy over EN24 Medium Carbon Steel by Friction Surfacing Using Different Mechtrode Diameter," e-Journal of Surface Science and Nanotechnology, 17, pp. 83-94.
https://doi.org/10.1380/ejssnt.2019.83

[10] Gandra, J., Pereira, D., Miranda, R. M., and Vilaça, P., 2013, "Influence of process parameters in the friction surfacing of AA 6082-T6 over AA 2024-T3," Procedia CIRP, 7, pp. 341-346.
https://doi.org/10.1016/j.procir.2013.05.058

[11] Galvis, J. C., Oliveira, P. H. F., Hupalo, M. F., Martins, J. P., and Carvalho, A. L. M., 2017, "Influence of friction surfacing process parameters to deposit AA6351-T6 over AA5052-H32 using conventional milling machine," Journal of Materials Processing Technology, 245, pp. 91-105.
https://doi.org/10.1016/j.jmatprotec.2017.02.016

[12] Nixon, R. G. S., Mohanty, B. S., and Bhaskar, G. B., 2018, "Effect of process parameters on physical measurements of AISI316 stainless steel coating on EN24 in friction surfacing," Materials and Manufacturing Processes, 33(7), pp. 778-785.
https://doi.org/10.1080/10426914.2017.1388524

[13] Rafi, H. K., Ram, G. J., Phanikumar, G., and Rao, K. P., 2010, "Friction surfaced tool steel (H13) coatings on low carbon steel: A study on the effects of process parameters on coating characteristics and integrity," Surface and Coatings Technology, 205(1), pp. 232-242.
https://doi.org/10.1016/j.surfcoat.2010.06.052

[14] Kumar, B. V., Reddy, G. M., and Mohandas, T., 2014, "Identification of suitable process parameters for friction surfacing of mild steel with AA6063 aluminium alloy," The International Journal of Advanced Manufacturing Technology, 74(1-4), pp. 433-443.
https://doi.org/10.1007/s00170-014-5964-7

[15] Seidi, E., Miller, S. F., and Carlson, B. E., 2021, “Friction Surfacing Deposition by Consumable Tools," Journal of Manufacturing Science and Engineering, 143(12), 120801. https://doi.org/10.1115/1.4050924

[16] Sekharbabu, R., Rafi, H. K., and Rao, K. P., 2013, “Characterization of D2 tool steel friction surfaced coatings over low carbon steel,” Materials & Design, 50, pp. 543-550. https://doi.org/10.1016/j.matdes.2013.03.042

[17] Puli, R., and Ram, G. J., 2012, “Wear and corrosion performance of AISI 410 martensitic stainless steel coatings produced using friction surfacing and manual metal arc welding,” Surface and Coatings Technology, 209, pp. 1-7. https://doi.org/10.1016/j.surfcoat.2012.06.075

[18] Li, H., Qin, W., Galloway, A., and Toumpis, A., 2019, “Friction surfacing of aluminium alloy 5083 on DH36 steel plate,” Metals, 9(4), 479. https://doi.org/10.3390/met9040479

[19] Pereira, D., Gandra, J., Pamies-Teixeira, J., Miranda, R. M., and Vilaça, P., 2014, “Wear behaviour of steel coatings produced by friction surfacing,” Journal of Materials Processing Technology, 214(12), pp. 2858-2868. https://doi.org/10.1016/j.jmatprotec.2014.06.003

[20] Rafi, H. K., Ram, G. J., Phanikumar, G., and Rao, K. P., 2011, “Microstructural evolution during friction surfacing of tool steel H13,” Materials & Design, 32(1), pp. 82-87. https://doi.org/10.1016/j.matdes.2010.06.031

[21] Guo, D., Kwok, C. T., Tam, L. M., Zhang, D., and Li, X., 2020, “Hardness, microstructure and texture of friction surfaced 17-4PH precipitation hardening stainless steel coatings with and without subsequent aging,” Surface and Coatings Technology, 402, 126302. https://doi.org/10.1016/j.surfcoat.2020.126302

[22] Gandra, J., Pereira, D., Miranda, R. M., Silva, R. J. C., and Vilaça, P., 2013, “Deposition of AA6082-T6 over AA2024-T3 by friction surfacing-Mechanical and wear characterization,” Surface and Coatings Technology, 223, pp. 32-40. https://doi.org/10.1016/j.surfcoat.2013.02.023

[23] Galvis, J. C., Oliveira, P. H. F., Martins, J. D. P., and Carvalho, A. L. M. D., 2018, “Assessment of process parameters by friction surfacing on the double layer deposition,” Materials Research, 21(3), e20180051. https://doi.org/10.1590/1980-5373-mr-2018-0051

[24] Troysi, F., Silva, K., Santos, Í. D., and Brito, P., 2019, “Investigation of Austenitic Stainless Steel Coatings on Mild Steel Produced by Friction Surfacing Using a Conventional CNC Machining Center,” Materials Research, 22(2), e20180301. https://doi.org/10.1590/1980-5373-mr-2018-0301

[25] Silva, K. H. S., Brito, P. P., Santos, I. B., Câmara, M. A., and Abrão, A. M., 2020, “The behaviour of AISI 4340 steel coatings on low carbon steel substrate produced by friction surfacing,” Surface and Coatings Technology, 399, 126170. https://doi.org/10.1016/j.surfcoat.2020.126170

[26] Seidi, E., and Miller, S. F., 2020, “Friction surfacing from radial surface of A6063 aluminum alloy consumable tool onto A36 carbon steel,” Proceedings of the ASME 2020 International Mechanical Engineering Congress and Exposition, Volume 2A: Advanced Manufacturing, Virtual, Online, V02AT02A003. https://doi.org/10.1115/IMECE2020-23502

[27] Seidi, E., and Miller S. F., 2020, “A Novel Approach to Friction Surfacing: Experimental Analysis of Deposition from Radial Surface of a Consumable Tool,” Coatings, 10(11), 1016. https://doi.org/10.3390/coatings10111016

[28] MatWeb: Online Materials Information Resource, Accessed April 12, 2021, Available from: www.matweb.com.